Available online at www.sciencedirect.com
ScienceDirect
Trans. Nonferrous Met. Soc. China 31(2021) 3050−3062
Transactions of Nonferrous Metals Society of China
www.tnmsc.cn

Process optimization, microstructures and mechanical/thermal properties of Cu/Invar bi-metal matrix composites fabricated by spark plasma sintering

Qiang-qiang NIE[1], Guo-hong CHEN[2], Bing WANG[3,4], Lei YANG[5], Wen-ming TANG[1,6]

1. School of Materials Science and Engineering, Hefei University of Technology, Hefei 230009, China;
2. Electric Power Research Institute, State Grid, Anhui Electric Power Co., Ltd., Hefei 230601, China;
3. The 43 Research Institute of China Electronics Technology Group Corporation, Hefei 230088, China;
4. Anhui Province Key Laboratory of Microsystem, Hefei 230088, China;
5. Hefei Shengda Electronic Technology Industry Co., Ltd., Hefei 230088, China;
6. Engineering Research Center of High-performance Copper Alloy Materials and Processing, Ministry of Education, Hefei 230009, China

Received 19 December 2020; accepted 31 March 2021

Abstract: An orthogonal experiment scheme was designed to investigate the effects of the Cu content, compaction pressure, and sintering temperature on the microstructures and mechanical and thermal properties of (30−50)wt.%Cu/Invar bi-metal matrix composites fabricated via spark plasma sintering (SPS). The results indicated that as the Cu content increased from 30 to 50 wt.%, a continuous Cu network gradually appeared, and the density, thermal conductivity (TC) and coefficient of thermal expansion of the composites noticeably increased, but the tensile strength decreased. The increase in the sintering temperature promoted the Cu/Invar interface diffusion, leading to a reduction in the TC but an enhancement in the tensile strength of the composites. The compaction pressure comprehensively affected the thermal properties of the composites. The 50wt.%Cu/Invar composite sintered at 700 °C and 60 MPa had the highest TC (90.7 W/(m·K)), which was significantly higher than the TCs obtained for most of the previously reported Cu/Invar composites.

Key words: spark plasma sintering (SPS); Cu/Invar bi-metal composite; microstructure; interface diffusion; mechanical property; thermal property

1 Introduction

The continuous shift of electronic devices toward miniaturization, portability, and multi-functionalization has necessitated the development of electronic packaging materials with high thermal conductivities (TC) and tensile strengths as well as low coefficients of thermal expansion (CTE) that match those of the Si and GaAs semiconductor chips in the electronics [1]. Undoubtedly, Cu metal is an ideal packaging material due to its extremely high TC and its excellent processing, electroplating, and soldering properties [2,3]. However, a severe CTE mismatch exists between Cu and the semiconductor chips or the ceramic substrates. Moreover, Cu is relatively weak and has a low softening point, which causes Cu plates, cases, and leads to become easily and permanently deformed during the thermal sealing process of the devices. To overcome these property deficiencies, the Invar alloy FeNi32Co4, with an extremely low CTE of only 0.4×10^{-6} K^{-1} (RT−200 °C) [4], can be combined with Cu to form Cu/Invar bi-metal

Corresponding author: Wen-ming TANG, Tel: +86-551-62901362, E-mail: wmtang@hfut.edu.cn
DOI: 10.1016/S1003-6326(21)65714-X

composites, which feature high TCs derived from the Cu and low CTEs and high tensile strengths derived from the Invar alloy, giving the composites excellent processing, electroplating, and soldering performance [5].

Since both Cu and the Invar alloy have a face-centered cubic (fcc) structure and similar lattice parameters, interdiffusion between Cu and the Invar alloy is favorable at high temperatures, giving rise to compositional changes of the materials upon mixing. Dissolution of the Fe and Ni atoms, in particular the Fe atoms, leads to lattice distortion and increases electron scattering within Cu. As a result, the TC of Cu rapidly decreases [6,7]. Meanwhile, the compositional changes result in a loss of the Invar effect in the Invar alloy [8], which reduces the ability of the Invar alloy to inhibit the thermal expansion of Cu. It was previously reported by WANG et al [9] that a 45wt.%Cu/Invar alloy composite prepared by vacuum arc melting and exsolution aging had a CTE as low as 8.72×10^{-6} K^{-1} (RT−300 °C) but a rather low TC (41.53 W/(m·K)) as a result of the high Fe and Ni composition in Cu (17 wt.%). In our previous research [10], we found that a 40wt.%Cu/Invar composite fabricated by pressureless sintering and thermomechanical treatment processes exhibited a TC of only 25.42 W/(m·K) due to the significant Cu/Invar interface diffusion. The Cu/Invar interfacial diffusion was accelerated at the temperatures above 700 °C [11]. Therefore, in order to mitigate interface diffusion and, therefore, improve the thermal properties of the Cu/Invar composites, sintering must be executed at temperatures as low as possible.

Spark plasma sintering (SPS) process has been known to achieve more rapid sintering densification at a lower temperature than traditional sintering methods [12,13]. Accordingly, SPS has been successfully used to prepare material comprising ultrafine and even nano-sized crystals. A dense Cu bulk with an average grain size of 0.5−3 μm and a low-expansion $Fe_{59}Ni_{36}Cu_5$ alloy (5.2×10^{-6} K^{-1} (RT−295 °C)) with an average grain size of 30 nm were produced via SPS [14,15]. Furthermore, the SPS is highly effective for restraining the interfacial diffusion/reaction of the composites. For example, the GNF/Al interface reaction in graphite nanoflakes GNFs/6061Al matrix composites fabricated by SPS was prevented without the formation of any harmful Al_4C_3. The resulting composites demonstrated a satisfactory TC of 155 W/(m·K) in the direction perpendicular to the loading axis [16].

SPS is believed to play an important role in suppressing interface diffusion, optimizing the microstructures, and improving the mechanical/thermal properties of Cu/Invar bi-metal composites. However, to date, research on the fabrication of the composites via SPS has not been reported. In this work, an orthogonal experiment scheme was designed to optimize the SPS process parameters, such as Cu content, sintering temperature, and compaction pressure, of Cu/Invar bi-metal composites using the TC, CTE and tensile strength of the composites as indices. The interface characteristics and the relationships between the microstructures, as well as the mechanical and thermal properties, of the composites were investigated to provide guidance for developing novel Cu/Invar electronic packaging composites with high TC and strength and low CTE.

2 Experimental

2.1 Materials

The spherical gas-atomized Cu powder (99.8 wt.% purity and an average particle size below 38 μm) and super Invar alloy powder (99.9 wt.% purity with a particle size of 23−75 μm) were employed as raw materials. The composition of the super Invar alloy powder is listed in Table 1.

Table 1 Chemical composition of gas-atomized super Invar alloy powder (wt.%)

Ni	Co	C	O	Fe
31.92	3.84	0.013	0.03	Bal.

2.2 Processing

The Cu and Invar powders were added to a nylon tank in mass ratios of 30:70, 40:60, and 50:50. After milling for 10 h in a FT−20 type pot mill, the powder mixtures were annealed at 400 °C for 1 h in an OTF−1200X type tube furnace to remove the surface oxides. The entire process was conducted under a 99.99 vol.% high-purity hydrogen atmosphere. Then, the powder mixtures were transferred to a graphite die with an inner diameter of 25 mm and sintered in a Labox−350 type SPS furnace. The sintering parameters are

listed in a non-standard L9 (3^3) orthogonal table (Table 2). The effects of the Cu content, compaction pressure, and sintering temperature on the microstructures and mechanical/thermal properties of the Cu/Invar composites were systematically studied to obtain the optimal SPS parameters. The entire sintering process was carried out under vacuum (<10 Pa) at an average heating rate of 100 °C/min and a holding time of 1 min. After sintering, the sample was cooled to room temperature in the SPS chamber, and the axial load was then removed.

Table 2 Factors and levels of orthogonal experiment scheme

Level	Factor		
	A (Compaction pressure/MPa)	B (Sintering temperature/°C)	C (Cu content/ wt.%)
1	40	700	30
2	50	750	40
3	60	800	50

2.3 Characterization

After the Cu/Invar composite samples were ground and polished, the distributions of the Cu and Invar components were observed using a MR2000 type light microscope (LM). The microstructures of the composites were investigated using a SU8020 type field-emission scanning electron microscope (FE-SEM), and the microzone elemental distributions in the composites were analyzed by an Oxford INCA type energy dispersive spectrometer (EDS). More detailed structural information at the Cu/Invar interface of the composites was investigated using a JEM−2100F type transmission electron microscope (TEM). Prior to TEM testing, a *d*3 mm × 200 μm circular sheet was cut from the composites. After grinding to a thickness of 50 μm, the sample was recessed to a thickness about 10 μm and then was continuously reduced using a Gatan−691 type ion beam thinner until it was perforated. The phases of the Cu/Invar composites were determined by X-ray diffraction (XRD, X'Pert PRO MPD-type X-ray diffractometer) with Cu K_α radiation (λ=0.154 nm) at a scanning rate of 2 (°)/min over a 2θ angle range of 10°−90° as well as a tube voltage and current of 20 kV and 200 mA, respectively.

The density of the Cu/Invar composite sample was determined by the Archimedes method. The tensile strength (R_m) of the composites was evaluated using an MX−0580 type small load microcomputer-controlled testing instrument at a beam displacement rate of 3 mm/min. Square-shaped samples with a gauge length of 5 mm and cross-sectional area of 1.5 mm × 1.5 mm were employed for tensile strength testing [17]. The tensile fracture morphologies of the samples were observed by FE-SEM. The length variation (ΔL) of the composite samples (3 mm × 4 mm × 8 mm) was measured using a TMA402F3 type thermal mechanical analyzer, and the average linear expansion coefficient (α) was calculated [18] based on Eq. (1) as

$$\alpha=\frac{1}{L_0}\frac{\Delta L}{\Delta T} \tag{1}$$

where L_0 is the original length of the sample at room temperature, and ΔT is the temperature range during the measurements (RT−100 °C). The measurements were carried out under a 99.9 vol.% purity N_2 atmosphere at a flow rate of 20 mL/min and a heating rate of 5 °C/min. The coefficient of thermal diffusion (a) of the Cu/Invar composites with dimensions of *d*6 mm × (2−3) mm was measured with a LFA457 laser thermal conductivity analyzer. The TC (λ) of the composites was calculated as

$$\lambda=a\rho c_p \tag{2}$$

where ρ is the density (g/cm^3), and c_p is the specific heat at constant pressure (J/(g·K)) of the composites. The c_p values of Cu and the Invar alloy are 0.39 and 0.515 J/(g·K) [19], respectively, and the c_p of the Cu/Invar composites was calculated via the rule of mixtures [20].

3 Results and discussion

3.1 Orthogonal experiments

The extreme R values used as indices of the relative density, TC, CTE and tensile strength of the Cu/Invar composites obtained from the orthogonal experiment are listed in Table 3. When the relative density of the composites was indexed, the effect strength of the factors is in the order of C (Cu content) > A (compaction pressure) > B (sintering temperature). The similar R values obtained indicated that sintering densification of the composites was not controlled by a single factor but

Table 3 Results of orthogonal experiments

Number		Factor			Relative density/%	CTE/ ($10^{-6}K^{-1}$)	TC/ ($W\cdot m^{-1}\cdot K^{-1}$)	$R_{p0.2}$/ MPa	R_m/ MPa
		A	B	C					
1		1	1	2	95.6	10.7	58.4	182	284
2		1	2	3	96.2	12.1	87.8	176	274
3		1	3	1	95.4	10.1	35.2	220	313
4		2	1	1	94.2	8.6	40.2	176	284
5		2	2	2	97.1	10.4	58.8	190	290
6		2	3	3	97.2	12.3	84.2	234	312
7		3	1	3	97.5	11.5	90.7	191	300
8		3	2	1	95.8	8.9	38.6	211	329
9		3	3	2	98.6	11.3	52.7	211	330
Relative density	$\overline{K}_1$	95.7	95.8	95.1					
	$\overline{K}_2$	96.2	96.4	97.1					
	$\overline{K}_3$	97.3	97.1	97.1					
	R	1.6	1.3	2.0					
TC	$\overline{K}_1$	60.5	63.1	38.0					
	$\overline{K}_2$	61.1	61.7	56.6					
	$\overline{K}_3$	60.7	57.4	87.6					
	R	0.6	5.7	49.6					
CTE	$\overline{K}_1$	10.9	10.3	9.2					
	$\overline{K}_2$	10.4	10.5	10.0					
	$\overline{K}_3$	10.6	11.2	10.7					
	R	0.5	0.9	1.5					
R_m	$\overline{K}_1$	291	289	306					
	$\overline{K}_2$	295	294	301					
	$\overline{K}_3$	316	318	295					
	R	25	29	11					

Note: $\overline{K}_i$ is the average value of the relevant index under a certain factor at level i, R is the difference between the maximum value and the minimum value of $\overline{K}_i$ for a certain factor

rather by multiple factors. Based on the observed trend in the $\overline{K}_i$ values, the degree of densification of the composites increased as the sintering temperature, compaction pressure, and Cu content all increased. Since the mechanical properties of the composites are closely related to their densities, the tensile strength of the Cu/Invar composites increased with higher compaction pressure and sintering temperature. The tensile strength of the composites decreased with increasing Cu content due to the higher tensile strength of the Invar alloy (400 MPa) [21] compared to that of the sintered Cu (230 MPa in this work). A comparison of the R values of the composites demonstrated that the sintering temperature had a significantly higher impact on the tensile strength of the composites than both the compaction pressure and Cu content.

When the TC of the composites was indexed, the resulting R values were very highly correlated to the Cu content (approximately 9.6 and 16.5 times higher than the R values of the sintering temperature and compaction pressure, respectively). The $\overline{K}_i$ value increased with decreasing sintering temperature and increasing Cu content. However,

as the compaction pressure increased, the $\bar{K}_i$ value first increased and then decreased. The final factor indexed was the CTE of the composites, which indicated that the $\bar{K}_i$ value increased with increasing sintering temperature and Cu content. Additionally, as the compaction pressure increased, the $\bar{K}_i$ value first decreased and then increased. Accordingly, stronger composites were obtained after sintering at higher temperatures. The optimized SPS process used was A3B3C1 (60 MPa, 800 °C, 30 wt.% Cu). Using the TC of the composites as the index for evaluating the quality of the composites, the process was changed to A2B1C3 (50 MPa, 700 °C, 50 wt.% Cu). However, using the CTE of the composites as the index, the optimal SPS process was determined to be A2B1C1 (50 MPa, 700 °C, 30 wt.% Cu).

As indicated in Tables 4 and 5, the Cu content had a stronger effect on the TC and CTE indices than did the sintering temperature and compaction pressure. When the tensile strength was the index, the Cu content, sintering temperature, and compaction pressure all influenced each other, and no single factor dominated. However, as shown in Table 6, the sintering temperature had the strongest effect on the R_m as the index (Table 6). Therefore, the subsequent analysis of the microstructures and properties of the Cu/Invar composites focused on the sintering temperature and Cu content.

Table 4 Variance analysis of results for TC as index

Factor	Sum of squares	Degree of freedom	Mean square	*F*	*P*
A	0.56	2	0.28	0.18	<0.1
B	53.81	2	26.9	16.92	<0.05
C	3760.93	2	1880.46	1182.68	>0.05
Error	3.17	2	1.59		

Note: $F0.1(2, 2)=9.00$, $F0.05(2, 2)=19.00$; F=(average of sum of squares of deviations)/(average of mean square error); $P<0.1$ indicates that the F value is smaller than $F0.1(2, 2)$ when the significance level α is 0.1, while $P>0.05$ indicates that the F value is larger than $F0.05(2, 2)$ when α is 0.05.

Table 5 Variance analysis of results for CTE as index

Factor	Sum of squares	Degree of freedom	Mean square	*F*	*P*
A	0.46	2	0.23	2.3	<0.1
B	1.56	2	0.78	7.8	<0.1
C	11.58	2	5.79	57.9	>0.05
Error	0.2	2	0.1		

Table 6 Variance analysis of results for R_m as index

Factor	Sum of squares	Degree of freedom	Mean square	*F*	*P*
A	1112	2	556	9.58	<0.05
B	1462	2	731	12.6	<0.05
C	168	2	84	1.45	<0.1
Error	116	2	58		

3.2 Microstructures

Based on the XRD patterns of the Cu/Invar composites fabricated by SPS at different temperatures and pressures in Fig. 1(a), the composites were mainly composed of Cu and the fcc γ-Invar. However, the body-centered cubic (bcc) α-Fe(Ni) was also detected around 44.5° (Fig. 1(b)). As the sintering temperature and compaction pressure increased, the intensities of the α-Fe(Ni) peaks and those of the γ-Invar peaks gradually increased and decreased, respectively. This was mainly attributed to the compositional change of the

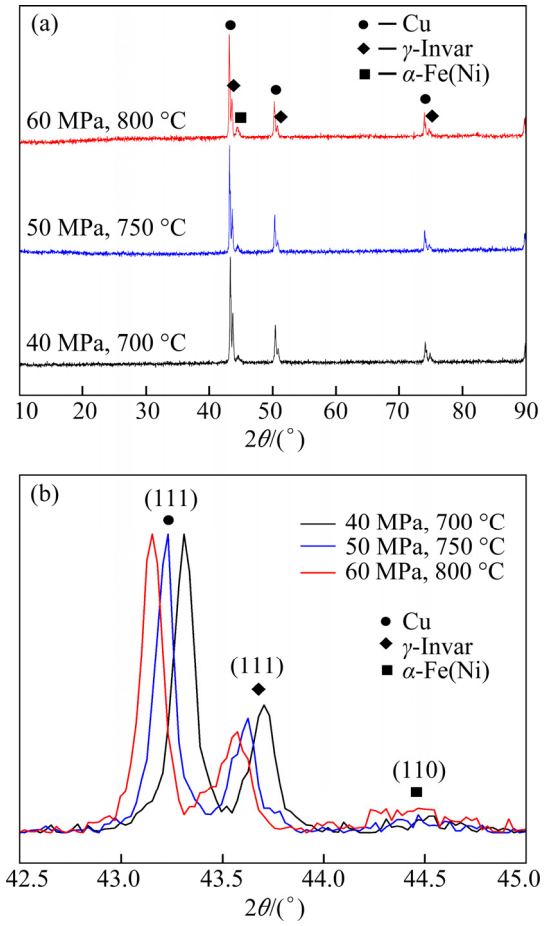

Fig. 1 XRD patterns (a) and magnified view of 2θ= 42.5°−45° region (b) of 40wt.%Cu/Invar composites sintered at different temperatures and pressures

Invar alloy due to the Cu/Invar interface diffusion during the SPS process. It is well-known that an infinite Cu(Ni) solid solution exists in the Cu−Ni binary system; however, in the Cu−Fe binary system, the solid solubility of Fe in Cu was only 1.1 wt.% at 850 °C [6]. Therefore, the diffusion of the Ni atoms from the Invar alloy into Cu during the sintering process was more significant than that of the Fe atoms, resulting in a reduction in the Ni content in the Invar alloy particles. When the Ni and Co content was less than 30 wt.%, the Invar alloy changed from an fcc arrangement (γ-Invar) to a bcc arrangement to form the α-Fe(Ni) phase [22]. In this study, as the compaction pressure and sintering temperature increased, the large plastic deformation of the components within the composites caused the Cu/Invar interface area to increase, accelerating the Cu/Invar interface diffusion. Thus, it was clear that more γ-Invar was converted to α-Fe(Ni).

The Cu (111) and γ-Invar (111) diffraction peaks of the 40wt.%Cu/Invar composites shifted slightly to a lower reflection angle orientation as the sintering temperature and compaction pressure both increased (Fig. 1(b)). Because the atomic radius of Cu (1.28 Å) is slightly larger than both Fe (1.24 Å) and Ni (1.25 Å), the diffusion of the Cu atoms through the Invar alloy caused the Invar alloy lattice to expand in volume. After SPS, the cooling rate of the sample reached 100 °C/min, which induced a high residual thermal stress in the composites. Due to the large CTE difference between the sintered pure Cu ($17\times10^{-6}\,K^{-1}$, RT−100 °C) [9] and the Invar alloy [4], the Cu matrix in the composites was subjected to residual tensile stress during the rapid cooling process, inducing Cu lattice expansion. As a result, the Cu diffraction peaks of the composites also shift slightly lower reflection angle orientation.

As shown in Fig. 2, the Invar alloy in the composites was not fully densified during the sintering process at 700 °C due to its high melting point (approximately 1450 °C) [6], leading to the presence of several small pores in the Invar alloy. The 30wt.%Cu/Invar composite had the highest concentration of the Invar alloy, which was continuously distributed throughout the composite, while the Cu matrix was segmented and randomly filled in the voids in the Invar alloy matrix. Therefore, the 30wt.%Cu/Invar composite exhibited

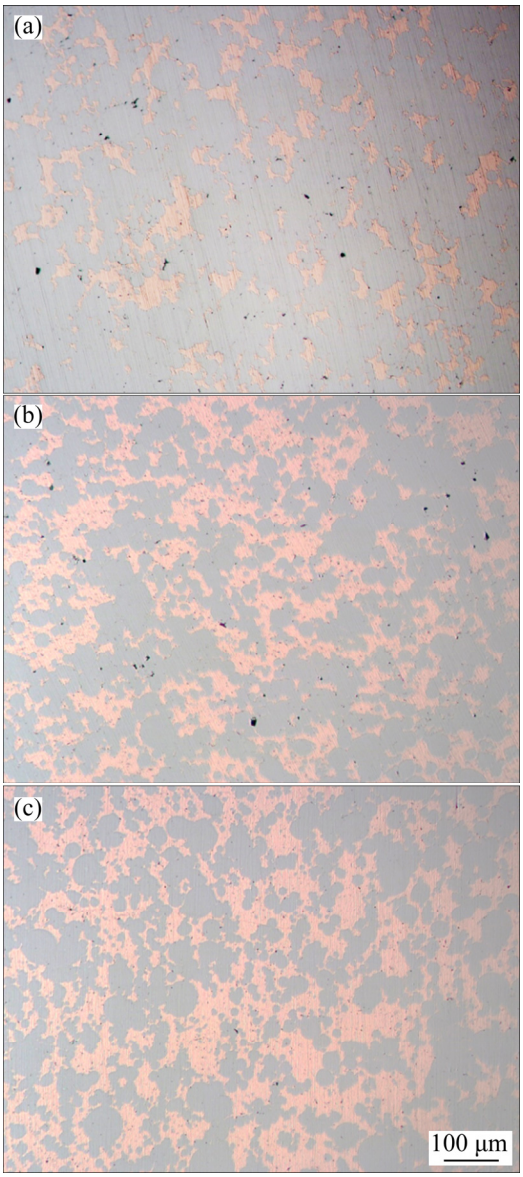

Fig. 2 LM cross-sectional images of Cu/Invar composites sintered at 700 °C: (a) A2B1C1, 50 MPa, 30 wt.%; (b) A1B1C2, 40 MPa, 40 wt.%; (c) A3B1C3, 60 MPa, 50 wt.%

the highest porosity and the lowest density of the other composites with different Cu contents, even though it was sintered under a high compaction pressure (50 MPa) (Fig. 2(a)). As the Cu content in the composite increased, the particles in the Invar alloy within the composites became increasingly less aggregated, which decreased the size of the pores in the composites. Therefore, the density of the composites gradually increased (Figs. 2(b, c)). On the other hand, in the 50wt.%Cu/Invar composite, Cu acted as the continuous matrix in which the Invar alloy particles were distributed

discontinuously. This composite had the highest density, the smallest pore size, and the lowest porosity of them all (Fig. 2(c)).

The interface characteristics of the 40wt.%Cu/Invar composite sintered at different sintering temperatures and compaction pressures were elucidated using SEM coupled with EDS (Fig. 3). In the composite obtained using the A1B1C2 conditions (40 MPa, 700 °C, 40 wt.% Cu), the Cu matrix was dense and featured very few pores (Fig. 3(a)). In addition, the Cu/Invar interface was sharp, and no interface layer was detected by EDS, indicating that the Cu/Invar interface diffusion was not apparent after sintering at 700 °C. As the sintering temperature increased, the thickness of the interfacial diffusion zone increased, reaching approximately 1.5 μm in the composite sintered at 800 °C (Fig. 3(c)), which was consistent with the Cu/Invar lamellar composites sintered at 800 °C for 1 h [23].

To more clearly identify the interface structure, the Cu/Invar composite fabricated using the A1B1C2 conditions was chosen for TEM analysis. As shown in Fig. 4(a), the Cu/Invar interface was continuous and tightly bounded, and atom interdiffusion across the interface barely occurred. From the high-resolution TEM (HRTEM) micrograph (Fig. 4(b)), the thickness of the Cu/Invar interface was determined to be less than 5 nm. The interplanar distances within the Cu and Invar alloy were approximately 2.09 Å and 2.08 Å, respectively, which were equal to the same interplanar distances of Cu (111) (2.086 Å, PDF70-3039) and Invar (111) (2.074 Å, PDF47-1405). In addition, no lattice distortion was observed, confirming that the Cu/Invar interface diffusion was completely inhibited in the composites sintered at 700 °C.

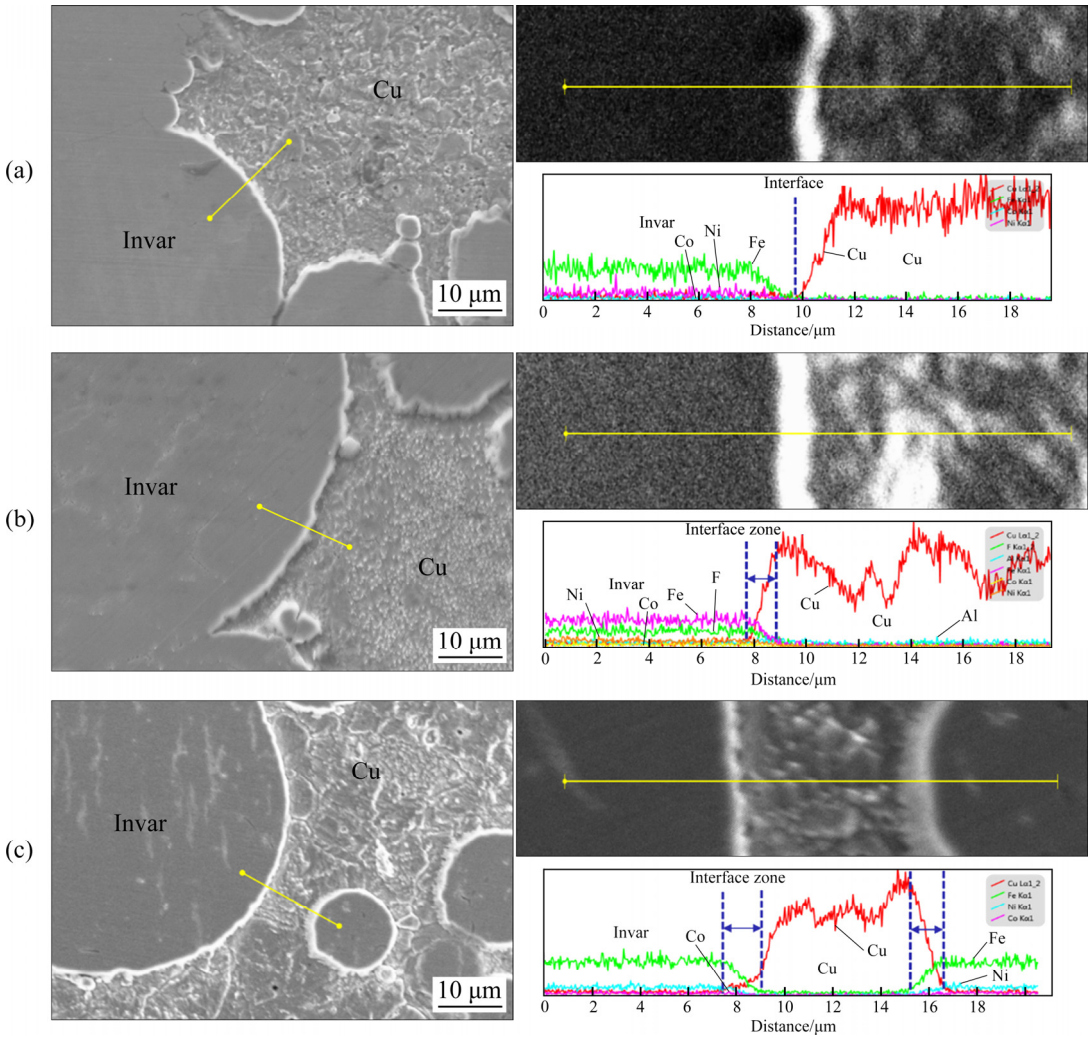

Fig. 3 SEM cross-sectional images and EDS linear scanning curves of 40wt.%Cu/Invar composites sintered at different temperatures and pressures: (a) A1B1C2, 40 MPa, 700 °C; (b) A2B2C2, 50 MPa, 750 °C; (c) A3B3C2, 60 MPa, 800 °C

3.3 Tensile strength and fracture morphology

As shown in Fig. 5(b), the R_m of the Cu/Invar composite fabricated under the A1B1C2 conditions was the lowest (284 MPa) compared to the composites fabricated under the other conditions but was still higher compared to the sintered pure Cu (230 MPa). As the sintering temperature and compaction pressure increased, the R_m values of the composite both increased, with the Cu/Invar composite fabricated under the A3B3C2 conditions being the highest R_m (330 MPa), mainly due to the improved densification (Fig. 5(a)) and the enhanced Cu/Invar interface bonding (Fig. 3).

As shown in Fig. 6, under a uniaxial tensile load, the fracture of the 40wt.%Cu/Invar composite samples depended predominantly on the tearing of the Cu matrix, following a typical dimple aggregation-type fracture mechanism. Pores and cracks were observed among the granular Invar alloy particles on the fracture surface of the 40wt.%Cu/Invar composite (A1B1C2) (Fig. 6(a)), which indicated that the sintering temperature and compaction pressure were both too low to achieve full densification of the Invar alloy. The fracture cracks in the Invar alloy propagated preferentially along the pores and the Invar particle boundaries. As the compaction pressure and sintering temperature increased, the size and quantity of the pores in the Invar alloy decreased (Figs. 6(b, c)), reflecting the high degree of sintering densification of the Invar alloy. Meanwhile, the Cu/Invar interface bonding strength also increased through atom interdiffusion. Due to the very large difference in $R_{p0.2}$ between Cu and Invar alloy in the composite (60 and 340 MPa, respectively) [24], plastic deformation occurred overwhelmingly in the Cu matrix until it fractured under a tensile load. The proportion of the Cu ductile fracture surface in the whole fracture surface of the composites increased continuously (Figs. 6(b, c)). In addition, during the

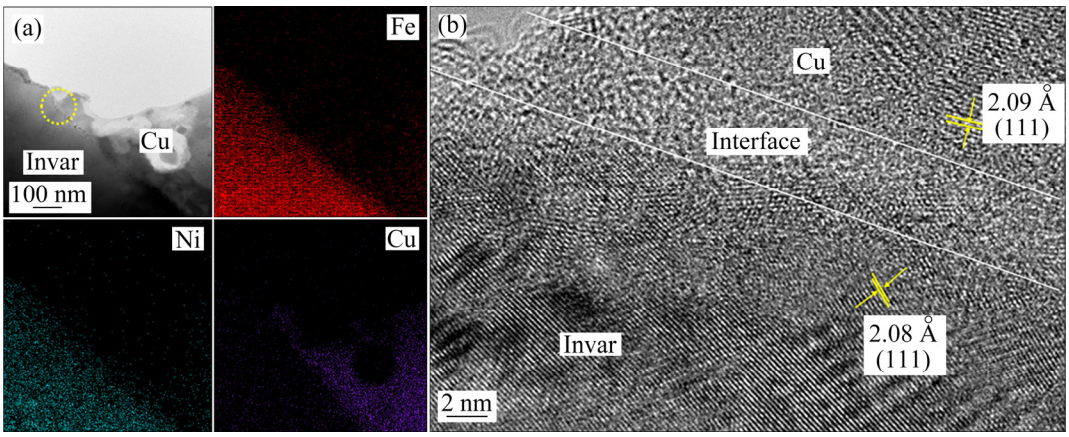

Fig. 4 Interface structure and elemental mappings of Cu/Invar composite sintered under condition of A1B1C2 (40 MPa, 700 °C, 40 wt.%) (a), and HRTEM micrograph (b) of circle area in (a)

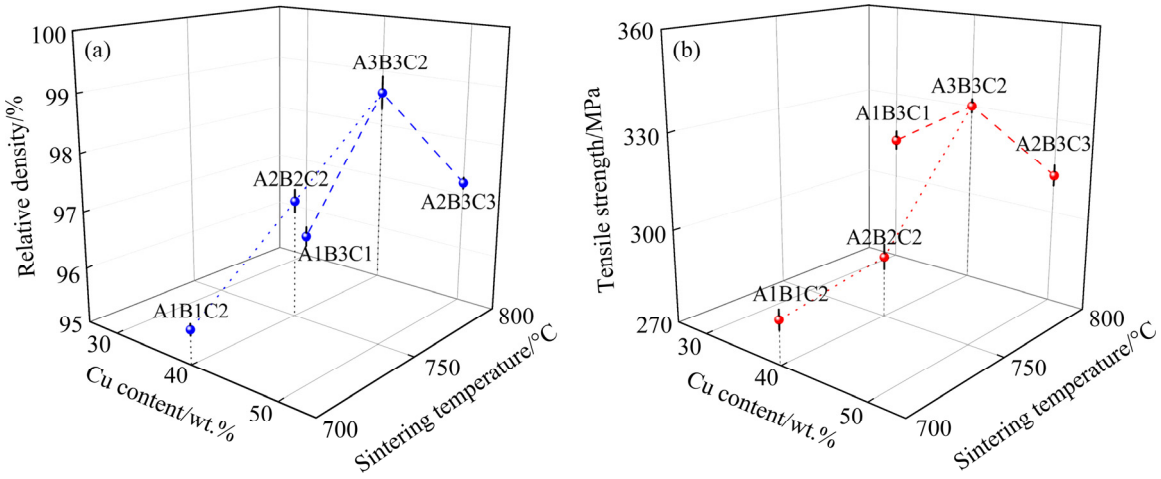

Fig. 5 Relative density (a) and tensile strength (b) of Cu/Invar composites prepared under different conditions

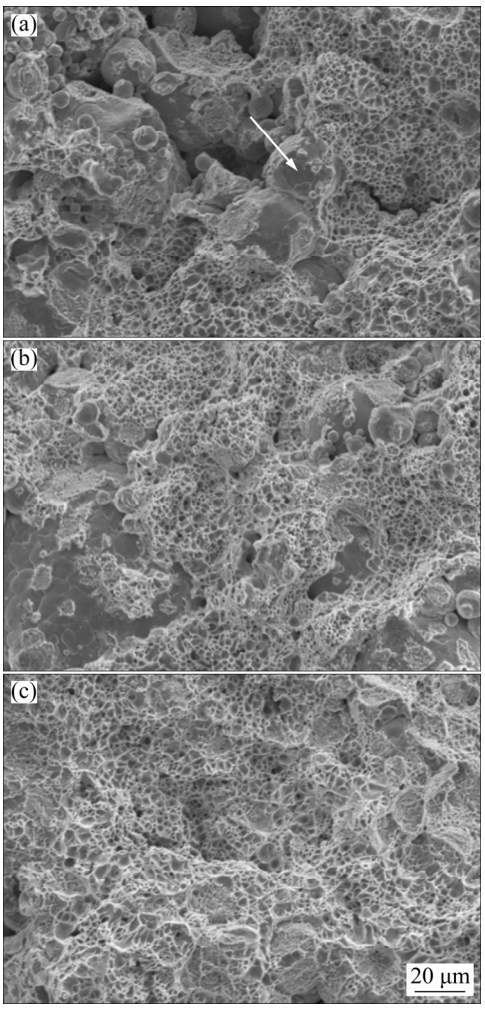

Fig. 6 SEM images showing fracture surfaces of 40wt.%Cu/Invar composites prepared at different sintering temperatures and compaction pressures: (a) A1B1C2, 40 MPa, 700 °C; (b) A2B2C2, 50 MPa, 750 °C; (c) A3B3C2, 60 MPa, 800 °C

fracturing of the 40wt.%Cu/Invar composite sintered at 60 MPa and 800 °C, only tearing of the Cu matrix occurred (Fig. 6(c)).

3.4 Thermal conductivities

As mentioned above, the Cu content and the sintering temperature strongly influenced the TCs of the Cu/Invar composites. As shown in Table 3 and Fig. 7, the 50wt.%Cu/Invar composite sintered at 700 °C and 60 MPa exhibited the highest TC (90.7 W/(m·K)). As the Cu content in the composite decreased, the Invar alloy gradually distributed continuously, and the Cu/Invar interface also increased, while the TC of the composite decreased to 39.2 W/(m·K) (A2B1C1). It was previously reported that the resistivity of Cu increased by 9.2 μΩ·cm per 1 wt.% Fe atoms dissolved in the Cu

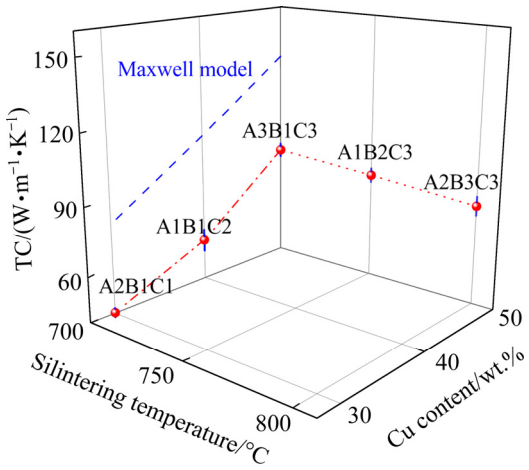

Fig. 7 Comparison of TCs obtained for Cu/Invar composites with values calculated using modified Maxwell model

matrix [25]. Comparably, the TC of the Cu−Fe alloy herein also correspondingly decreased with higher Fe contents. While an increase in the sintering temperature of the Cu/Invar composites improved the density, it also led to an increased interface diffusion and, therefore, a reduction in the TC of the composites. Furthermore, the increase in the compaction pressure increased both the densification and the interface bonding, thus enhanced the TC of the Cu/Invar composites. However, as the compaction pressure increased to 60 MPa, improvement in the interface bonding accelerated the interface diffusion of the Cu/Invar composites, which was deleterious to the TC of the composites. As a result, the mean TC value of the Cu/Invar composite first increased and then decreased with increasing compaction pressure (Table 3).

The TC of the Cu/Invar composites was predicted by the modified Maxwell model [16]:

$$K_c = K_m[\frac{K_r + (n-1)K_m - (n-1)V_r(K_m - K_r)}{K_r + (n-1)K_m + V_r(K_m - K_r)}] \quad (3)$$

where K_c, K_r, and K_m were TC values of the composite, the reinforcement (Invar) (12 W/(m·K)) [9], and the Cu matrix (328 W/(m·K), the measured value of pure Cu sintered by SPS at 700 °C in this work), respectively, and V_r and n were the volume fraction and shape factor of the reinforcement, with n being equal to 3 for the spherical Invar alloy particles [26]. Although the TC of the sintered Cu/Invar composites was significantly improved compared to those of

the composites fabricated by pressureless sintering [6,10], the empirical TC values were still lower than the corresponding theorical values calculated by the modified Maxwell model (Fig. 7). This was mainly due to the undesirable microstructures of the composites of the pores, Invar alloy agglomeration, and Cu/Invar interface. In future work, approaches such as optimization of the Invar alloy particle size and incorporation of the Ag interface barrier layer [20] should be explored to further improve the microstructures and properties of the Cu/Invar composites.

The TC values of the composites fabricated by SPS in this work were much higher than the those of the Cu/Invar composites fabricated via casting, pressureless sintering, extrusion molding, and chemical synthesis in previous works (Fig. 8). Although the Cu/Invar composites prepared by extrusion molding displayed the highest TC (120 W/(m·K)) in the extrusion direction, extrusion molding in the extrusion direction also leads to a violent plastic deformation of the composites, resulting in significant anisotropy of the microstructure and mechanical properties of the composites [30].

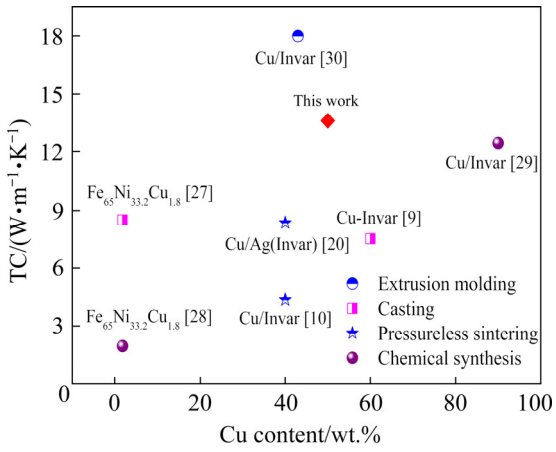

Fig. 8 TC values of various Cu/Invar composites prepared by different techniques

3.5 Coefficients of thermal expansion

Based on the results presented in Table 3, the Cu content and sintering temperature were the main factors affecting the CTE of the Cu/Invar composites, while the compaction pressure had the weakest effect. Because of the Invar effect, an increase in the Invar content strongly restricted the CTE of the composites. However, the Invar effect of the Invar alloy was highly sensitive to the elemental composition of the alloy [24]. During the SPS process, the Cu/Invar interface diffusion changed the elemental composition of the Invar alloy by reducing the Ni content, which, therefore, reduced Invar effect of the alloy. This phenomenon becomes more apparent as the sintering temperature of the composites increased during fabrication. As a result, the CTE of the composites increased gradually with the sintering temperature. In addition, as the compaction pressure increased from 40 to 50 MPa, both the relative density of the composites and the Cu/Invar interface bonding strength increased. The restricting effect of the Invar alloy on the thermal expansion of the Cu matrix was also amplified, leading to an effective decrease in the CTE of the Cu/Invar composites. However, as the compaction pressure increased to 60 MPa, the intensive plastic deformation of the Cu matrix and the Invar alloy increased in the interfacial area and the interface bonding, accelerating the diffusion across the Cu/Invar interface. It promoted the change in the elemental composition of the Invar alloy and the increase in the α-Fe(Ni) content, both of which manifested the increase in the CTE of the composites. Therefore, the 30wt.%Cu/Invar composite (A1B2C1) had the lowest CTE (8.6×10^{-6} K^{-1}, RT−100 °C).

The Turner and Kerner models are frequently used to predict the CTE of particle-reinforced metal matrix composites. The Turner model assumes that only uniform hydrostatic stress exists in the composites, neglecting their shear deformation, and is given by [31]

$$\alpha_c = \frac{\alpha_m V_m K_m + \alpha_p V_p K_p}{V_m K_m + V_p K_p} \tag{4}$$

The Kerner model assumes that the reinforced particles are wrapped uniformly by the metal matrix, and the normal stress and shear stress in the composites are taken into consideration as described by [32]

$$\alpha_c = \alpha_m V_m + \alpha_p V_p + V_p V_m(\alpha_p - \alpha_m)\cdot \frac{K_p - K_m}{V_m K_m + V_p K_p + 3/4(K_m K_p / G_m)} \tag{5}$$

$$K = \frac{E}{3(1-2\upsilon)} \tag{6}$$

$$G = \frac{E}{2(1+\upsilon)} \tag{7}$$

where α is the CTE, V is the volume fraction, K is

the volume modulus, G is the shear modulus, E is the elastic modulus, and v is the Poisson's ratio. The subscripts c, m, p represent the composite, matrix, and reinforcement, respectively. The data used in the above model calculations are listed in Table 7. As shown in Fig. 9, the measured CTEs of the composites were consistently higher than the theoretical values predicted by these two models, which could be explained by several reasons. First, the Invar effect is very sensitive to the elemental composition of the Invar alloy; therefore, a miniscule change in the composition of the Invar alloy could lead to a pronounced increase in the CTE of the Invar alloy [24]. In addition, the relative density and the Cu/Invar interface bonding strength of the composites sintered at 700 °C were so low that the ability for the Invar alloy to inhibit the thermal expansion of the Cu matrix was greatly reduced.

Table 7 Physical properties of Cu and Invar alloy employed in model calculations [9,33]

Sample	$\alpha/10^{-6}\ K^{-1}$	E/GPa	v	K/GPa	G/GPa
Cu	17	130	0.3	108	50
Invar alloy	0.5	145	0.24	93	58

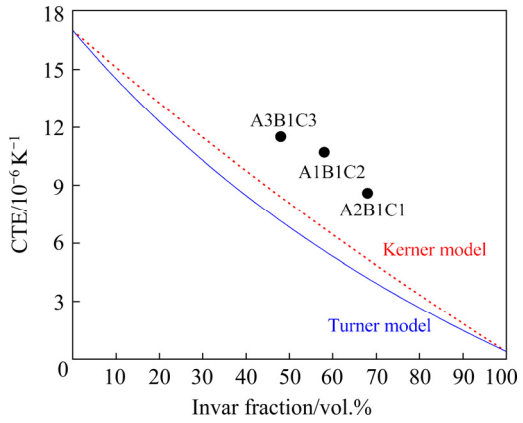

Fig. 9 Comparison of tested CTEs with model calculated results of Cu/Invar composites sintered at 700 °C

Moreover, Fig. 9 also indicated that the Kerner model was more suitable for predicting the CTE of the Cu/Invar composites than the Turner model. The deviation between the empirical CTEs and the theoretical values of the composites decreased with increasing compaction pressure and Cu content. This was due to the enhancement of the bonding at the Cu/Invar interface with increasing the compaction pressure. It was also observed that the increase in the Cu content of the composites led to a decrease in the aggregation degree of the Invar alloy as well as an improvement in the restraining effect of the Invar alloy on the thermal expansion of the Cu matrix.

4 Conclusions

(1) Taking the relative density and tensile strength as indices, the optimal processing parameters were determined to be a compaction pressure of 60 MPa, a sintering temperature of 800 °C, and a Cu content of 30 wt.%. Taking the TC as index, the optimal processing parameters are determined to be a compaction pressure of 50 MPa, a sintering temperature of 700 °C, and a Cu content of 50 wt.%. Taking the CTE as the index, the optimal processing parameters were determined to be a compaction pressure of 50 MPa, a sintering temperature of 700 °C, and a Cu content of 30 wt.%.

(2) In the Cu/Invar composites sintered via SPS at 700 °C, the Cu/Invar interface diffusion was almost completely inhibited. However, the bonding between Invar particles in the alloy was rather weak, which caused tensile fracture cracks to preferentially propagate within the Invar particles. As the sintering temperature increased, both the density and tensile strength of the Cu/Invar composites increased, leading to tensile fracture cracks that propagated in the Cu matrix following a dimple aggregation-type fracture mechanism.

(3) As the sintering temperature increased from 700 to 800 °C, the TC of the composites decreased, while the CTE increased. When the compaction pressure increased from 40 to 50 MPa, the degree of densification of the composites and the Cu/Invar interfacial bonding was enhanced, leading to an increase in the TC and a decrease in the CTE of the composites. As the compaction pressure further increased to 60 MPa, the Cu/Invar interfacial diffusion became more pronounced, which was not beneficial for improving the thermal properties of the composites.

Acknowledgments

The authors are grateful for the financial support from the International Science & Technology Cooperation Program of China (No. 2014DFA50860).

References

[1] CAI Hui, WANG Ya-ping, SONG Xiao-ping, DING Bing-jin. Research progress in copper matrix composites for electronic packaging [J]. Materials Review, 2009, 23: 24−28. (in Chinese)

[2] TAO Jing-mei, ZHU Xin-kun, TIAN Wei-wei, YANG Peng, YANG Hao. Properties and microstructure of Cu/diamond composites prepared by spark plasma sintering method [J]. Transactions of Nonferrous Metals Society of China, 2014, 24(10): 3210−3214.

[3] MIRAZIMI J, ABACHI P, PURAZRANG K. Microstructural characterization and dry sliding wear behavior of spark plasma sintered Cu−YSZ composites [J]. Transactions of Nonferrous Metals Society of China, 2016, 26(7): 1745−1754.

[4] BERTHOLD J W, JACOBS S F. Ultraprecise thermal expansion measurements of seven low expansion materials [J]. Applied Optics, 1976, 15(10): 2344−2347.

[5] JOHANNES W R, JOHNSON W. Controlling the coefficient of thermal expansion of printed wiring board using copper−Invar−copper foil [J]. International Journal of Microcircuits and Electronic Packaging, 1994, 17: 135−142.

[6] WU Dan, WU Shi-pu, YANG Lei, SHI Chang-dong, WU Yu-cheng, TANG Wen-ming. Preparation of Cu/Invar composites by powder metallurgy [J]. Powder Metallurgy, 2015, 58(2): 100−105.

[7] LIU Ya-jun, ZHANG Li-jun, DU Yong, SHENG Guang, WANG Jiang, LIANG Dong. Atomic mobilities, zero-flux planes and flux reversals in fcc Cu−Fe−Ni alloys [J]. Calphad, 2011, 35(3): 376−383.

[8] GORRIA P, BLANCO D M, BLANCO J A, HERNANDO A, GARITAONANDIA J S, BARQUÍN L F, CAMPO J, SMITH R I. Invar effect in fcc-FeCu solid solutions [J]. Physical Review B, 2004, 69: 214421.

[9] WANG Cui-ping, LE Fan-cheng, ZHU Jia-hua, YANG Mu-jin, YANG Shui-yuan, ZHANG Jin-bin, ISHIDA K, LIU Xing-jun**.** Microstructures and thermophysical properties of Cu−Fe64Ni32Co4 alloys [J]. Rare Metal Materials and Engineering, 2019, 48: 2122−2129.

[10] WU Dan, YANG Lei, SHI Chang-dong, WU Yu-cheng, TANG Wen-ming. Effects of rolling and annealing on microstructures and properties of Cu/Invar electronic packaging composites prepared by powder metallurgy [J]. Transactions of Nonferrous Metals Society of China, 2015, 25(6): 1995−2002.

[11] LI Bao-zeng, WANG Qing, WANG Ying-ming, LI Chun-yan, QIANG Jian-bing, JI Chun-jun, DONG Chuang. Cu-containing Fe−Ni corrosion-resistant alloys designed by a cluster-based stable solid solution model [J]. Metallurgical and Materials Transactions A, 2012, 43: 544−554.

[12] HU Zheng-yang, ZHANG Zhao-hui, CHENG Xing-wang, WANG Fu-chi, ZHANG Yi-fan, LI Sheng-lin. A review of multi-physical fields induced phenomena and effects in spark plasma sintering: Fundamentals and applications [J]. Materials and Design, 2020, 191: 108662.

[13] ROMARIC C, SOPHIE L G, FOAD N, FRÉDÉRIC C, GUILLAUME B, GILBERT F, MARC C J, FRÉDÉRIC B. Effect of current on the sintering of pre-oxidized copper powders by SPS [J]. Journal of Alloys and Compounds, 2017, 692: 478−484.

[14] ZHU K N, GODFREY A, HANSEN N, ZHANG X D. Microstructure and mechanical strength of near- and sub-micrometre grain size copper prepared by spark plasma sintering [J]. Materials and Design, 2017, 117: 95−103.

[15] PRICĂ C V, NEAMŢU B V, POPA F, MARINCA T F, SECHEL N, CHICINAŞ I. Invar-type nanocrystalline compacts obtained by spark plasma sintering from mechanically alloyed powders [J]. Journal of Materials Science, 2018, 53: 3735−3743.

[16] CHEN Guo-dong, CHANG Hao, SUN Jian, WANG Bing, YANG Lei, ZHANG Jian-hua, TANG Wen-ming. Microstructures and properties of graphite nanoflake/6061Al matrix composites fabricated via spark plasma sintering [J]. Journal of Materials Engineering and Performance, 2020, 29: 1235−1244.

[17] ZHANG L H, JIANG Y, FANG Q F, ZHANG T, WANG X P, LIU C S. Toughness and microstructure of tungsten fibre net-reinforced tungsten composite produced by spark plasma sintering [J]. Materials Science and Engineering A, 2016, 659: 29−36.

[18] NI J E, CASE E D, SCHMIDT R D, WU C I, HOGAN T P, TREJO R M, KIRKHAM M J, LARA-CURZIO E, KANATZIDIS M G. The thermal expansion coefficient as a key design parameter for thermoelectric materials and its relationship to processing-dependent bloating [J]. Journal of Materials Science, 2013, 48: 6233−6244.

[19] Matweb, Material properties data [DB/OL]. http://www.matweb.com/search/DataSheet.aspx?MatGUID=b6fb00b235f0442da4d31a0cd04671c9.

[20] ZHANG Xin, HUANG Ying-qiu, LIU Xiang-yu, YANG Lei, SHI Chang-dong, WU Yu-cheng, TANG Wen-ming. Microstructures and properties of the 40Cu/Ag(Invar) composites fabricated by powder metallurgy and subsequent thermo-mechanical treatment [J]. Metallurgical and Materials Transactions A, 2018, 49: 1869−1878.

[21] ZHAN Xiao-hong, LING Wan-li, GAO Qi-yu, YAN Ting-yan, LIU Zi-li. Microstructure and mechanical properties of the MLMPW on Invar alloy [J]. Materials Research Express, 2019, 6(4): 046529.

[22] ZHOU Y H, HARMELIN M, BIGOT J. Martensitic transformation in ultrafine Fe−Ni powders [J]. Materials Science and Engineering A, 1990, 124(2): 241−249.

[23] CHEN Peng, HUANG Hua-gui, JI Ce, ZHANG Xu, SUN Zhong-hua. Bonding strength of Invar/Cu clad strips fabricated by twin-roll casting process [J]. Transactions of Nonferrous Metals Society of China, 2018, 28(12): 2460−2469.

[24] COTTLE R D, CHEN X, JAIN R K, ELIEZER Z, RABENBERG L, FINE M E. Designing low-thermal-expansivity, high-conductivity alloys in the Cu−Fe−Ni ternary system [J]. JOM, 1998, 50: 67−69.

[25] SUN Bao-de, GAO Hai-yan, WANG Jun, SHU Da. Strength of deformation processed Cu−Fe−Ag in situ composites [J]. Materials Letters, 2007, 61: 1002−1006.

[26] XU J Z, GAO B Z, KANG F Y. A Reconstruction of Maxwell Model for Effective Thermal conductivity of

composite materials [J]. Applied Thermal Engineering, 2016, 102: 972−979.

[27] KHAN S A, ZIYA A B, LBRAHIM A, ATIQ S, AHMAD N, BASHIR F. The enhanced range of temperature for coefficient of low thermal expansion, electrical and thermal conductivities of Cu substituted Fe−Ni invar alloys [J]. Physica Scripta, 2016, 91: 035701.

[28] AHMAD S, ZIYA A B, ASHIQ M N, IBRAHIM A, ATIQ S, AHMAD N, SHAKEEL M, KHAN M A. Improved magnetic and electrical properties of Cu doped Fe−Ni invar alloys synthesized by chemical reduction technique [J]. Journal of Magnetism and Magnetic Materials, 2016, 419: 125−130.

[29] STOLK J, MANTHIRAM A. Chemical synthesis and properties of nanocrystalline Cu−Fe−Ni alloys [J]. Materials Science and Engineering B, 1999, 60(2): 112−117.

[30] JHA S. Cuvar—A new controlled expansion, high conductivity material for electronic thermal management [C]//Proceedings of the 45th Electronics Components and Technology Conference. Las Vegas, NV, 1995: 542−547.

[31] TURNER P S. Thermal expansion stresses in reinforced plastics [J]. Journal of Research of the National Bureau of Standards, 1946, 37: 239−250.

[32] CHANG Hao, SUN Jian, CHEN Guo-hong, WANG Bing, YANG Lei, ZHANG Jian-hua, TANG Wen-ming. Microstructure and properties of high-fraction graphite nanoflakes/6061Al matrix composites fabricated via spark plasma sintering [J]. Transactions of Nonferrous Metals Society of China, 2015, 31(6): 1550−1560.

[33] NIE Qiang-qiang, WEI Xin, QIN Xiao-long, HUANG Ying-qiu, CHEN Guo-hong, YANG Lei, TANG Wen-ming. Microstructure and properties of graphite nanoflakes/Cu matrix composites fabricated by pressureless sintering and subsequent thermo-mechanical treatment [J]. Diamond Related Materials, 2020, 108: 107948.

放电等离子体烧结 Cu/Invar 双金属基复合材料的工艺优化、显微结构与力学/热性能

聂强强[1]，陈国宏[2]，汪 冰[3,4]，杨 磊[5]，汤文明[1,6]

1. 合肥工业大学 材料科学与工程学院，合肥 230009；
2. 国网安徽省电力有限公司 电力科学研究院，合肥 230601；
3. 中国电子科技集团公司 第 43 研究所，合肥 230088；
4. 微系统安徽省重点实验室，合肥 230088；
5. 合肥圣达电子科技实业有限公司，合肥 230088；
6. 高性能铜合金材料及成形加工教育部工程研究中心，合肥 230009

摘 要：采用放电等离子体烧结(SPS)工艺制备(30~50)%Cu/Invar(质量分数)双金属基复合材料。通过设计正交实验方案，系统研究 Cu 含量、压制压力及烧结温度对复合材料显微结构、力学性能和热性能的影响。结果表明，随着 Cu 含量由 30%增加至 50%(质量分数)，Cu 基体逐渐转变为连续网络分布，复合材料致密度、热导率及热膨胀系数增大，但抗拉强度降低。提高烧结温度，Cu/Invar 界面扩散加剧，导致复合材料的热导率降低，抗拉强度增大。压力对复合材料热性能的影响较为复杂。在 700 °C，60 MPa 下制备的 50%Cu/Invar(质量分数)复合材料具有最高的热导率，为 90.7 W/(m·K)，优于以往报道的大多数 Cu/Invar 复合材料。

关键词：放电等离子体烧结(SPS)；Cu/Invar 双金属基复合材料；显微结构；界面扩散；力学性能；热性能

(Edited by Xiang-qun LI)